Wide Bicontinuous Compositional Windows from Co-Networks Made with Telechelic Macromonomers

Catherine N. Walker,[†] Kyle C. Bryson,[†] Ryan C. Hayward,[*,†] and Gregory N. Tew[*,†,‡]

[†]Department of Polymer Science & Engineering and [‡]Department of Veterinary and Animal Science, University of Massachusetts, Amherst, Massachusetts 01003, United States

ABSTRACT Phase-separated and self-assembled co-network materials offer a simple route to bicontinuous morphologies, which are expected to be highly beneficial for applications such as ion, charge, and oxygen transport. Despite these potential advantages, the programmed creation of co-network structures has not been achieved, largely due to the lack of well-controlled chemistries for their preparation. Here, a thiol−ene end-linking platform enables the systematic investigation of phase-separated poly(ethylene glycol) (PEG) and polystyrene (PS) networks in terms of the molecular weight and relative volume fractions of precursor polymers. The ion conductivity and storage modulus of these materials serve as probes to demonstrate that both phases percolate over a wide range of compositions, spanning PEG volume fractions from ∼0.3−0.65. Small angle X-ray scattering (SAXS) shows that microphase separation of these co-networks yields disordered structures with *d*-spacings that follow $d \sim M_n^{0.5}$, for 4.8 kg/mol < M_n < 37 kg/mol, where M_n is the molecular weight of the precursor polymers at the same ratio of PEG to PS. Over this range of molecular weights and corresponding *d*-spacings (22−55 nm), the ion conductivity ($10^{-4.7}$ S/cm at 60 °C), thermal properties (two glass transitions, low PEG crystallinity), and mechanical properties (storage modulus ≈90 MPa at 30 °C) remained similar. These findings demonstrate that this approach to thiol−ene co-networks is a versatile platform to create bicontinuous morphologies.

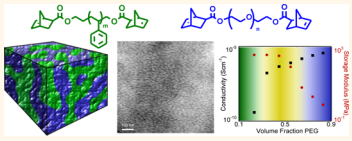

KEYWORDS: co-networks · bicontinuous morphology · thiol−ene · lithium ion conductivity · phase separation

Bicontinuous morphologies, which enable three-dimensional percolation of two different phases throughout the material, are especially advantageous as a route to concurrently incorporate seemingly contrasting properties that cannot be achieved using a single homogeneous material.[1] A good example is polymer membranes that require a highly mobile phase for efficient transport of a desired species and a simultaneously rigid phase to provide robust mechanical properties.[2] Despite their potential, bicontinuous morphologies are fundamentally difficult to obtain because they require variable curvature, high packing frustration, and large interfacial area.[3,4] Overcoming these morphological challenges to enable a consistent and broad bicontinuous compositional window will be advantageous for a variety of fields such as ion,[2,5,6] charge,[7] and oxygen transport[8] as well as water purification[2] and mechanical reinforcement of membranes.[9,10] A system with bicontinuous nanometer-scale phases would provide uninterrupted ion-conducting pathways, for example, while maintaining favorable mechanical properties, bypassing the geometric limitation demonstrated previously in solid electrolyte materials.[9,10]

Strategies to access bicontinuous morphologies on the nanoscale have predominantly fallen into two broad categories: those that take advantage of equilibrium self-assembly and those that limit demixing by kinetically trapping phase-separated structures. Equilibrium self-assembly of diblock copolymers has been widely studied in this context; however, bicontinuous structures such as the gyroid phase occupy only a narrow composition range of the phase diagram[11] and are therefore formed only under rigorously controlled conditions.[3,12,13] The bicontinuous gyroid geometry is characterized by varied curvature and high packing frustration that requires the block copolymer chains to stretch to fill space;[14] however, block copolymer melts prefer the constant curvature and low packing frustration found in the less complex lamellar and cylindrical phases.[12] These physical challenges limit the combinations of polymer chemistries, molecular weights,

* Address correspondence to rhayward@mail.pse.umass.edu, tew@mail.pse.umass.edu.

Received for review September 5, 2014 and accepted November 21, 2014.

Published online November 21, 2014
10.1021/nn505026a

and temperatures that lead to this desirable bicontinuous morphology.

To facilitate formation of bicontinuous morphologies, several variations on traditional diblock copolymers have been investigated. For example, ABA triblock copolymers with a polydisperse midblock were shown to have expanded windows of disordered bicontinuous morphologies due to the polydispersity of the midblock deceasing packing frustration.[15−18] However, the lamellar morphology continued to occupy a much larger compositional range than the bicontinuous morphology, and weak dependence of the *d*-spacing on the total molecular weight of the block copolymer makes it difficult to control domain size in this way.[15,16] Similarly, for ternary blends of two homopolymers and a compatibilizing graft-copolymer, polydisperse molecular weight and graft density of the copolymers was shown to widen the window in which disordered bicontinuous structures are formed,[19] compared to the narrow window obtained for diblock copolymer compatibilizers.[20,21]

An alternative strategy to increasing polydispersity is greatly increasing the number of blocks to form multiblock chains. This approach enhances the likelihood of obtaining the bicontinuous phase[22,23] since multiblock chains face barriers to the formation of ordered structures.[22,24,25] Disordered bicontinuous phases from multiblock copolymers have demonstrated improved mechanical properties including higher stress and strain at break compared to analogous triblock copolymers.[23,26] Often, multiblock copolymer synthesis requires a series of rigorous living polymerizations,[27−29] although recent investigations using end-linking strategies have simplified multiblock synthesis.[23,26,30]

In contrast to equilibrium structures, numerous groups have investigated methods to trap nonequilibrium bicontinuous morphologies formed as a result of spinodal decomposition.[31−34] Demixing is typically induced through solvent-,[35] temperature-,[36] or polymerization-induced[37,38] phase separation, and coarsening of the bicontinuous morphology is then kinetically arrested using several routes including vitrification,[32] chemical cross-linking,[39] or jamming/gelation of nanoparticles.[40] Some of these strategies are synthetically quite simple and have been used to generate nanoporous materials[41] as well as ion-conducting membranes with high modulus.[37,38] However, due to the delicate interplay between the kinetics of demixing and structural arrest, obtaining bicontinuous structures typically requires rigorously controlled processing conditions that are highly specific to a given chemical system.

Here, a third approach is considered that has received far less attention, namely, cross-linking two or more polymers in a homogeneous solution or blend, followed by the formation of microphase separated structures by changes in temperature or removal of solvent. Early studies predicted this approach[42] would lead to microphase separation with a domain spacing (*d*) that can be tuned by the molecular weight between cross-links (M_c) according to $d \sim M_c^{0.5}$, which was confirmed by neutron scattering.[43] However, in these early studies, the morphology was not determined and the possibility of bicontinuous phases was not explicitly discussed.[42,43] Later studies confirmed that the presence of random cross-links frustrates the formation of highly ordered phases,[44] resulting in disordered bicontinuous structures under appropriate conditions.[45−48] However, these studies have relied on random copolymerization of monomers with a telechelic macromonomer as a cross-linker, leading to uncontrolled network architectures.[45−49] Furthermore, bicontinuity has most commonly been established through measurements of the swelling ratios in water and nonpolar solvents, which can be complicated to interpret due to the possibility for solvent-induced structural rearrangements.[45−48] Other networks use block copolymers of various lengths to achieve a more defined architecture, yet these studies still rely heavily on swelling or AFM for their morphology characterization.[50−52]

While these approaches have generated important insights and numerous specific material systems that yield cocontinuous structures, a simpler and more universal route that is widely tolerant to variations in temperature, degree of polymerization, interaction strengths, and processing conditions will have broad implications and is expected to provide excellent model systems for fundamental investigations. One of the many areas that will benefit from facile synthesis of bicontinuous morphologies is the ability to improve and tailor the mechanical properties of solid electrolytes. Solid electrolytes, such as salt-loaded poly(ethylene glycol) (PEG), conduct ions *via* a series of chain relaxations; therefore, a trade-off exists between ion conductivity and robust mechanical properties.[6] Thus far, this trade-off has largely been investigated using equilibrium phase-separated, block copolymers of PEG with polystyrene (PS), *e.g.*, as studied by Balsara and co-workers.[5,53−55] These materials had a shear modulus of approximately 100 MPa, demonstrating that the mechanical properties are dictated by the polystyrene phase.[53] The major drawback to this strategy is that ion conductivity is limited by grain orientation; any lamellar grains aligned perpendicular to the applied voltage act as barriers to the ion conductivity. A bicontinuous morphology would overcome this drawback by ensuring that pathways for conductivity are uninterrupted in all directions.[5]

To address these broad challenges, we demonstrate that bicontinuous morphologies can be accessed over a wide compositional window by the microphase-separation of co-networks formed by high yielding

thiol−ene chemistry using end-functionalized polymer chains. The material consists of salt-loaded, ion-conducting PEG domains and mechanically reinforcing PS domains. Using the mechanical properties and Li-ion conductivity of the materials as probes to determine the connectivity of each phase, we demonstrate the existence of a wide bicontinuous phase window from ~30% to 65% by volume of PEG. Variation of the precursor polymer molecular weight (M_n) furthermore allows for controlled variations in the length-scale of the cocontinuous structure while retaining the advantageous combination of modulus and conductivity provided by the two microphases.

RESULTS AND DISCUSSION

Design and Synthesis. Our approach to co-networks is based on ultraviolet-light-initiated, random end-linking of two different norbornene-end-functionalized telechelic polymers, which provides a direct and efficient method to explore the conditions that lead to bicontinuous morphologies. Cross-linking is performed in a good solvent for both chains, presumably yielding random connections of precursor polymer chains at each network junction. Previously, this strategy has been used to give well-defined networks as demonstrated by their resilience at high strain and uniform neutron scattering in the swollen state.[56−58]

TABLE 1. Precursor Polymer and Network Properties

M_n PS [recursor (kg/mol)[a]	M_n PEG [recursor (kg/mol)[a]	*d*-spacing (nm)[b]	PEG crystalline fraction[c]
4.8	4.6	22 ± 2	~0
12	12	31 ± 1	0.07
37	35	55 ± 2	0.25

[a] As indicated by supplier. Throughout the text, network samples are identified by the PS molecular weight. [b] Domain spacing from primary peak SAXS. [c] Fraction of crystalline PEG compared to theoretical heat of fusion for PEG.

PEG and PS were chosen as model co-network components for several reasons. Many studies on PS−PEG block copolymers have been reported, and their phase behavior is well-known.[59] Also, PEG is a key polymer involved in lithium ion conductivity studies, and impedance spectroscopy is used here as a probe to demonstrate continuity of the PEG phase. Previously, PEG and PDMS were used to generate conducting membranes through a similar approach; however, these materials were soft (~0.1 MPa) due to the rubbery PDMS domains, and their morphologies were not determined.[60] As a result, PS was employed for the current study to increase stiffness and provide a means to assess percolation of the nonpolar phase. To study the ability to vary the length-scale of microphase separated structures, three different molecular weights were chosen, corresponding to values of M_n for PS of 4.8, 12, and 37 kg/mol, with nearly identical molecular weights of PEG (Table 1). The 4.8 kg/mol network was chosen as it falls near the predicted boundary for microphase separation of PS−PEO diblock copolymers[61] of $\chi N = 10.5$, while the upper end of 37 kg/mol was chosen because the end functionalization and thiol−ene chemistry became less efficient with increasing molecular weight, making it difficult to obtain high-quality networks. For example, 50 kg/mol PDMS networks have been synthesized by this technique;[62] however the gel fraction of 0.4 was significantly lower than those reported here.

Full synthetic details are provided in the Supporting Information. Briefly, Mitsunobu-type chemistry was used to end-functionalize each of the PEG and PS precursor polymers of different molecular weights with norbornene. This chemical handle allowed for cross-linking with a tetrafunctional thiol using a UV-light-initiated reaction as illustrated in Figure 1. Prior to any measurements, samples were thoroughly dried for approximately 3 days under nitrogen flow, then in a vacuum oven at 120 °C

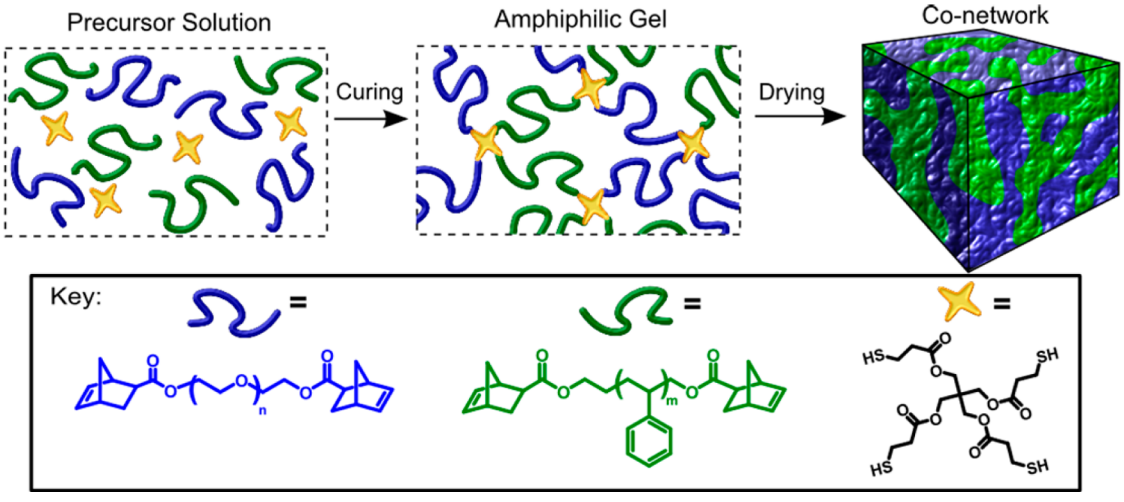

Figure 1. General scheme for obtaining salt-loaded co-network samples from norbornene end-functionalized precursor polymers.

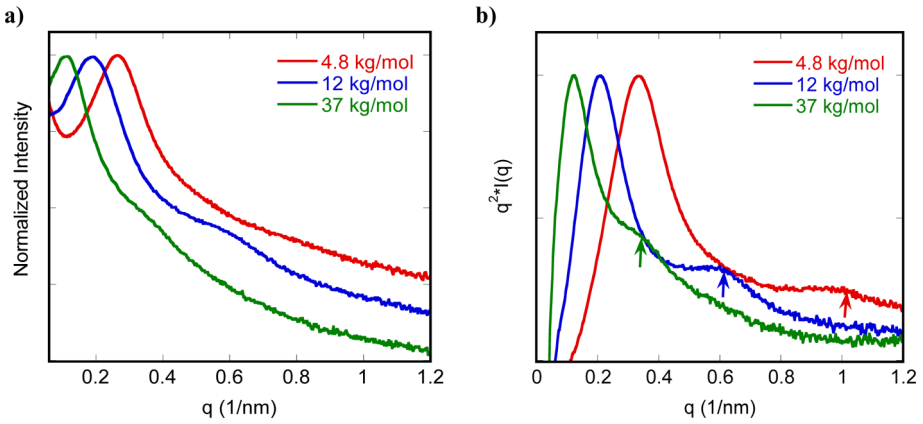

Figure 2. SAXS data in (a) intensity plot and (b) Kratky plot. Samples showed increasing *d*-spacing with increasing molecular weight and the higher order reflections, marked with arrows in (b), correspond to approximately 3*q.**

overnight. Norbornene was chosen for end functionalization because it is one of the most reactive enes for thiol–ene chemistry due to the release of ring strain and low probability of homopolymerization.[63,64] The cross-linker was chosen because of its four mercaptopropionate ester groups which are considered the most reactive thiol group because of their ability to form a six-membered hydrogen-bonded ring.[65] The interactions between the thiol protons and the carbonyl groups weaken the S–H bond and aid in forming the thiyl radicals.[65]

For each network, the desired masses of PEG and PS were dissolved in a common solvent (DMF) along with lithium bis(trifluoromethanesulfonylimide) (LiTFSI) at a molar ratio of 1:10 relative to PEG repeat units. After UV curing, the common solvent was thoroughly evaporated to yield salt-loaded, microphase-separated, co-network samples. The volume fraction of salt-loaded PEG in each network was calculated from the masses of each polymer used to prepare the network, and the density of 100% salt-loaded PEG and PS networks were determined using a pycnometer in hexane. A series of samples with varying molecular weight and nearly symmetric composition (ϕ_{PEG} = 0.55) was first studied to establish the formation of bicontinuous morphologies with a range of characteristic sizes. To determine the compositional boundaries of the bicontinuous phase, the 12 kg/mol precursor polymers were next studied over the range of ϕ_{PEG} = 0.23–0.83.

Morphology. The microphase separated structures of network samples with nearly symmetric compositions (ϕ_{PEG} = 0.55) and molecular weights varying from M_n = 4.8–37 kg/mol were first investigated using SAXS. As seen in Figure 2a, each sample shows a clear scattering peak with a *d*-spacing that increases with M_n. Well-ordered morphologies, typically observed in annealed block copolymer samples, are not expected here because random network connectivity frustrates the formation of long-range order. Given the nearly equal volume fractions of the two phases, and the modest contrast in chain stiffness, the microphase-separated

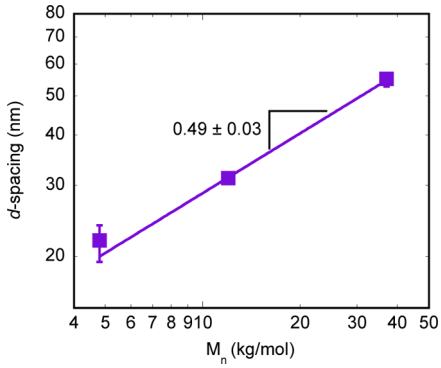

Figure 3. Scaling relationship between M_n and *d*-spacing closely follows the relationship predicted by de Gennes of $d \sim M_c^{0.5}$. The line is a best-fit power law with an exponent of 0.49 ± 0.03. Error bars represent the maximum and minimum of three independent measurements or the distribution of measurements is smaller than the symbol.

structure must presumably be a disordered bicontinuous phase. Notably, a secondary reflection, at approximately 3*q** is observed for each sample, as seen more clearly in the Kratky plot in Figure 2b. Similar scattering features have been observed in other bicontinuous disordered systems such as amphiphilic co-networks,[45] morphologies obtained by spinodal decomposition,[66] kinetically trapped phases,[38] and polydisperse triblocks.[15,17] It has been proposed that the presence of the 3*q** peak and absence of the 2*q** peak arises from morphologies with weakly ordered lamellar phases, where the length scale of an ordered grain is only a few times greater than the *d*-spacing.[45] As shown in Figure 3, the domain spacing ($d = 2\pi/q^*$) increases with M_n, in a manner consistent with the prediction by de Gennes of $d \sim M_c^{0.5}$ for a blend with cross-links introduced in the melt state.[42] The same scaling has been observed in other disordered, bicontinuous phase-separated systems.[44] Here, cross-links are introduced in a good solvent, where the polymer chains are swelled relative to their unperturbed melt dimensions. However, since the solutions are above the overlap concentration, the

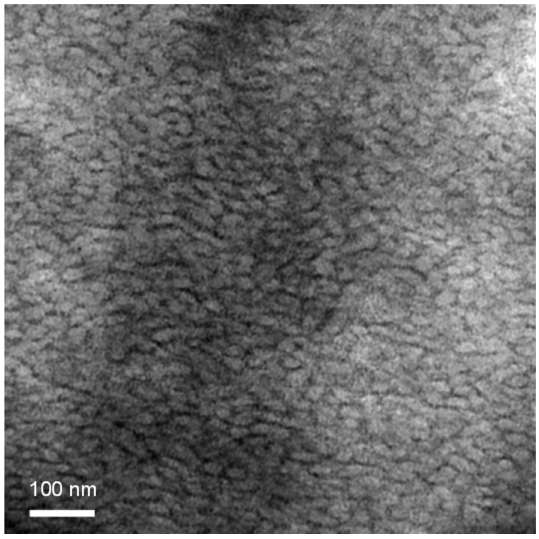

Figure 4. TEM image of the 12 kg/mol network. The PEG domains, stained with RuO_4, appear dark. The presence of disordered domains with a characteristic size-scale of 30 nm is consistent with the SAXS pattern.

end-to-end distance of the chains should still follow $M^{0.5}$, and hence, it is reasonable that the *d*-spacing of the microphase separated networks exhibits the same relationship.

A representative TEM image for the 12 kg/mol system (Figure 4) reveals a disordered structure with a domain spacing of ~30 nm, consistent with the SAXS result. The PEG domains, which appear darker due to preferential staining by RuO_4, are clearly interconnected, while the PS domains are somewhat extended, though perhaps not continuous. From this image (as from any two-dimensional slice through a three-dimensional morphology), it is difficult to make any firm conclusions about cocontinuity, but the presence of extended domains of both phases is at least consistent with a disordered cocontinuous structure, as has been reported for a number of other material systems.[15,17,38,45,66]

With respect to phase separation of these networks, it is important to consider the molecular weight and χ value for PEG–PS which is <0.1.[67] For a diblock copolymer,[61] the 4.8 kg/mol network should be near the limit of microphase separation of χN = 10.5 predicted by mean field theory. Randomly cross-linked networks require a higher value of χN for microphase separation compared to diblock copolymers,[42,43] suggesting that this lowest molecular weight co-network should be phase-mixed; however, this network was clearly phase-separated at room temperature as demonstrated by SAXS and up to 100 °C as demonstrated by differential scanning calorimetry (DSC) and dynamic mechanical analysis (DMA), as shown later. This is likely due to the presence of LiTFSI within the PEG domains, which increases the effective χ value for the system,[53,54,68,69] driving microphase separation even for this relatively low molecular weight.

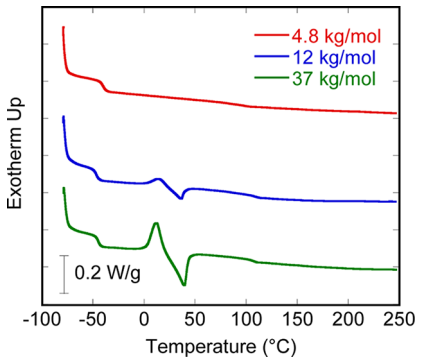

Figure 5. DSC measurements show that the LiTFSI loading effectively reduces crystallinity in the PEG phase. All data were taken from the second heating scan at a rate of 10 °C/min. Curves are offset for clarity.

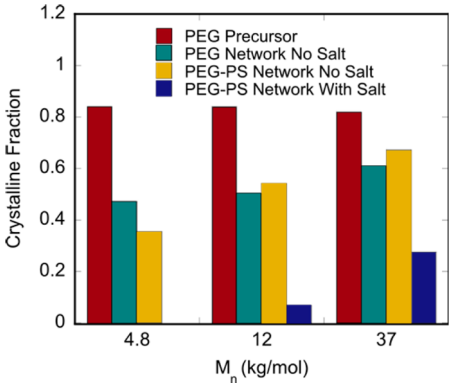

Figure 6. Crystalline fraction of PEG precursors, PEG networks without salt, PEG–PS networks without salt and PEG–PS networks with salt.

Thermal Properties. All of the salt-loaded PEG–PS networks are thermally stable up to 350 °C according to thermal gravimetric analysis as shown in Figure S8 (Supporting Information). DSC measurements (see Figure 5) demonstrate that the networks have limited crystallinity compared to the theoretical maximum heat of fusion for PEG. In the 4.8 kg/mol network, there was no crystallinity within the detection limit of this technique. The 12 and 37 kg/mol networks have approximately 7 and 28% crystalline PEG phases, respectively, despite the 10:1 EO/Li salt concentration. The melting temperature also increases slightly with M_n; the 12 kg/mol network melts at 36 °C, while the 37 kg/mol network melts at 39 °C. Additionally, no endothermic peak was observed at the reported melting temperature of the LiTFSI salt, approximately 230 °C, demonstrating that the salt is highly dissociated within the PEG phase.

In an effort to better understand how network chemistry impacts overall properties, PEG precursor polymers, 100% PEG networks, and PEG–PS networks without salt were also analyzed by DSC. The crystallinity of these samples is compared to the PEG–PS salt-loaded networks in Figure 6. The three PEG precursor polymers (red) had similar amounts of crystallinity (0.82–0.84, see Figure S9, Supporting Information),

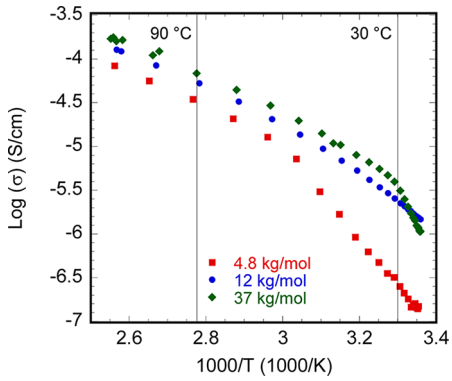

Figure 7. Impedance spectroscopy measurements show that the three networks have similar conductivity values above 60 °C. 90 and 30 °C are marked for reference.

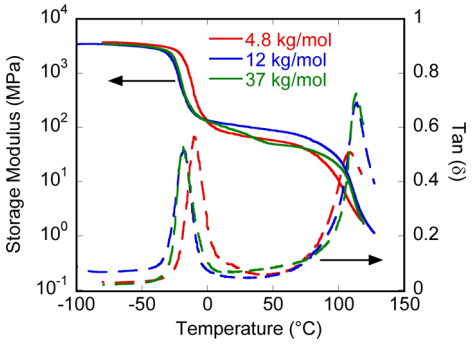

Figure 8. Dynamic mechanical analysis (DMA) measurements of storage modulus (left axis, solid lines) and tan δ (right axis, dashed lines) show each sample has two glass transitions (T_g's).

indicating that molecular weight has a minimal effect on crystalline fraction in these linear samples. However, the melting point showed a slight temperature dependence; the 4.8 kg/mol polymer melted at 51 °C, while the 12 kg/mol polymer melted at 57 °C and the 35 kg/mol polymer melted at 60 °C. In comparison, the 100% PEG networks (teal) also showed a slight M_n dependence in both crystalline fraction and melting temperature (Figure S10, Supporting Information). For this series, networks show a crystalline fraction between 0.47 and 0.61 that appears to increase slightly with M_n indicating that cross-linking the chains into a network decreases crystallinity compared to the linear precursor polymers. The melting points show a similar trend to the linear polymers. Introducing the polystyrene phase into the network (yellow) has little effect on the PEG crystallinity in the 12 and 35 kg/mol networks (Figure S11, Supporting Information). However, in the 4.8 kg/mol network, crystallinity decreases slightly. Finally, returning to the salt-loaded PEG–PS networks, it can be seen that the LiTFSI dramatically reduces PEG crystallinity. Yet, examining this series of networks (blue), it is observed that there is still a similar dependence on M_n to PEG–PS networks without salt (yellow) or PEG networks without salt (teal).

Ion Conductivity. Ion-conducting materials are of interest for solid electrolyte applications. Electrochemical impedance spectroscopy (EIS) was used here to measure ion conductivity (σ) as a probe to demonstrate that the salt-loaded PEG phase percolates throughout the sample. Figure 7 shows ion conductivities for networks of all three molecular weights to be approximately 10^{-5}–$10^{-4.5}$ S/cm at 60 °C, similar to other PEG-based materials.[70–72] Specifically, LiTFSI-loaded PEG–PS block copolymers with similar *d*-spacing, volume fraction, and salt loading (70 nm, ϕ_{PEG} = 0.54, and EO/Li = 12, respectively) have an ion conductivity of approximately 10^{-4} S/cm at 80 °C.[73] In the temperature range investigated, there was minimal evidence of crystallinity interfering with the ion conductivity. Only the 37 kg/mol network shows a pronounced downturn at low temperatures, consistent with DSC measurements indicating a higher degree of crystallinity in this sample. The networks with the higher M_n, 12 and 37 kg/mol, have slightly higher conductivities compared to the 4.8 kg/mol network especially below 60 °C. This could be due to the larger *d*-spacing, which contributes to wider ion-conducting pathways.[73]

Mechanical Properties. Mechanical properties were evaluated using DMA under tension of rectangularly shaped samples. The plots of storage moduli (E') and the loss tangents (tan δ) (Figure 8) show that each sample displays two glass transition temperatures (T_g's) as indicated by the temperature at which tan δ displays a local maximum. The PEG T_g's in each sample are between −20 and −10 °C, while the PS T_g's are between 107 and 112 °C. The low T_g and amorphous nature of the PEG phase allow for high ion conductivity, while the high T_g of the PS phase imparts mechanical rigidity. Between the two T_g's, E' is fairly stable with values of 50–90 MPa for the three networks, clearly indicating percolation of the stiff PS domains. These modulus values are much higher than those reported for typical PEG-based ion conducting materials,[70,74] and on par with some of the highest reported to date.[37,53] These values also show favorable comparison to commercial separators made of polytetrafluoroethylene or a composite of silica, alumina, and poly(ethylene terephthalate) that each showed a Young's modulus of approximately 60 MPa by nanoindentation.[75]

Volume Fraction Series. To assess the range over which bicontinuous structures are formed, a series of samples with varying ϕ_{PEG} were synthesized using the 12 kg/mol precursor polymers. Ion conductivity and storage modulus at 70 °C were compared across a wide range of volume fractions to assess whether both phases were percolated through the sample, as shown in Figure 9.

The ion conductivity shows a large step change of almost 3 orders of magnitude between ϕ_{PEG} = 0.23 and 0.32. In this region, even small changes in volume fractions, from 0.23 to 0.27, cause large differences in

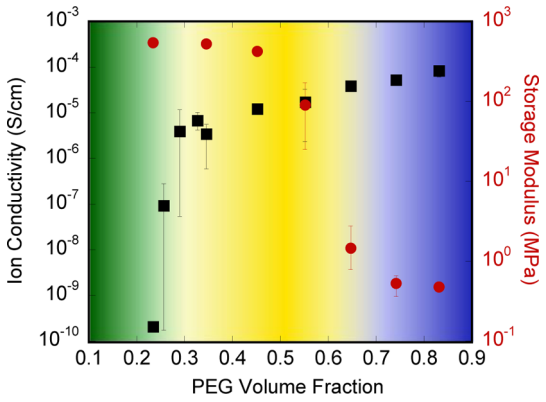

Figure 9. Ion conductivity and storage modulus versus PEG volume fraction series using 12 kg/mol precursor polymers at 70 °C. The green region highlights where only PS is continuous, the blue region depicts where only PEG is continuous, and the yellow region indicates where both phases are continuous. *Y*-axis error bars represent the maximum and minimum of three measurements. *X*-axis error bars also represent the range of three samples; however, these are smaller than the symbols.

ion conductivity. The $\phi_{PEG} = 0.23$ sample shows a conductivity approximately equivalent to the sensitivity of the instrument and is considered nonconducting. Above $\phi_{PEG} = 0.32$, ion conductivity increases more gradually, presumably because the structure has already become highly interconnected, and subsequent increases are largely due to the increasing volume fraction of PEG.

The difference in mechanical properties over the volume fraction series is evident from handling the samples at room temperature. Samples with $\phi_{PEG} < 0.4$ were rigid, brittle, and sometimes fractured during sample preparation. Samples with $\phi_{PEG} > 0.7$ were rubbery and sticky, also making them challenging to handle and cut to the desired geometry. Intermediate samples with similar amounts of PEG and PS were rigid enough to cut without deforming yet are not so brittle that they fractured. The storage modulus, as measured by DMA at 70 °C, confirmed these qualitative observations. For $\phi_{PEG} < 0.45$, the samples had a storage modulus above 500 MPa, a value rarely demonstrated in solid electrolytes. Even the network with $\phi_{PEG} = 0.55$ had a storage modulus of approximately 100 MPa. Networks with $\phi_{PEG} > 0.65$ had a much lower storage modulus of <1 MPa, which is similar to the 0.3 MPa of a 100% PEG network.[60]

Examining both measurements provides an estimate of the range of volume fractions over which the system is bicontinuous, as summarized in Figure 9. At the volume fraction where a percolated network is first formed, the respective property is expected to show a sharp increase above the characteristic value for a pure network of the majority phase. From the ion conductivity data, percolation appears to happen at $\phi_{PEG} \approx 0.25-0.3$, where the conductivity increases rapidly by orders of magnitude over the background value measured for more PS-rich samples. This region has been shaded in blue, see Figure S12 (Supporting Information), to highlight the volume fraction window for PEG percolation. Similarly, the storage modulus begins to increase sharply above the value for PEG rich networks around $\phi_{PEG} \approx 0.60-0.65$. The area shaded in green in Figure S13 (Supporting Information) highlights the volume fractions over which PS is likely continuous as evidenced by the high storage modulus. The overlay of these two supplemental figures is given in Figure 9, where the region in yellow indicates the simultaneous percolation of both PEG and PS phases. Samples toward the center of this region show PEG-like ion conductivities and PS-like storage moduli, indicating that both phases are highly interconnected, while those at either edge show a drop off in respective properties as a smaller portion of the minority phase forms part of the percolated network. The faded colors near the boundaries depict these numbers as our initial estimations. While further studies are required to better understand the evolution of morphology with composition, and more precisely define the bicontinuous phase boundaries, these results clearly demonstrate that disordered bicontinuous structured are formed across a wide range of compositions for these co-networks prepared by well-defined cross-linking reactions.

CONCLUSIONS

Here, we systematically investigated the formation of disordered bicontinuous morphologies in co-networks defined by a clean and efficient thiol−ene cross-linking platform. Changing the molecular weight between the precursor polymers allowed for control over the size of the microphase-separated domains, with bicontinuous morphologies accessible over a wide range of volume fractions, demonstrating the versatility of this system. Microphase separation in PEG/PS co-networks allowed us to simultaneously achieve high modulus and high ion conductivities. Consistent properties were found across the range of length scales probed, further demonstrating the versatility of this platform. Given the general utility of the Mitsunobu and thiol−ene reactions, we envision this strategy to be broadly applicable to many combinations of polymers and applications where bicontinuous morphologies are desirable, beyond the high-modulus, ion-conducting materials discussed here.

METHODS

Materials and Instruments. Three molecular weights of dihydroxyl-terminated poly(ethylene glycol) (PEG) [(Mn = 4.6 kDa, Đ = 1.03), (12) (35)] and polystyrene (PS) (M_n = 4.8 kDa, Đ = 1.14) (12) (37)], 5-norbornene-2-carboxylic acid (99% exo) (NB), triphenylphosphine (PPh3), diisopropyl azodicarboxylate

(DIAD), pentaerythritol tetrakis(3-mercaptopropionate) (4SH), 2-hydroxy-4′-(2-hydroxyethoxy)-2-methylpropiophenone (PI), tetrahydrofuran (THF), dichloromethane (DCM), methanol (MeOH), and ethyl ether were purchased from Alfa Aesar, Sigma-Aldrich, Acros Organics, and Polymer Source and used without further purification unless otherwise stated.

^{1}H NMR spectra were recorded at 300 MHz using a Bruker DPX-300 NMR spectrometer. Chemical shifts (δ) are reported in ppm and coupling constants (J) in Hertz. Gel permeation chromatography (GPC) was performed using Agilent 1260 series system with a PL gel 5 μm guard column, two 5 μm analytical Mixed C columns, and a 5 μm analytical Mixed D column (Agilent), incubated to 40 °C. THF was used as the eluent at a flow rate of 1.0 mL/min. Polystyrene standards were used for the calibration and toluene was used for the flow marker. Thermogravimetric analysis (TGA) measurements were taken using a TA Instruments TGA Q500 with a heating rate of 10 °C/min up to 600 °C under nitrogen. Differential scanning calorimetry (DSC) measurements were taken using a TA Instruments DSC Q200. Samples were analyzed using a heating rate of 10 °C/min under a flow of nitrogen (50 mL/min). Impedance measurements were performed using a Solatron 1260 impedance/gain phase analyzer in a Cascade TEK TVO-2 vacuum oven. SAXS patterns were obtained from an Osmic MaxFlux Cu Kα X-ray source with a wavelength of 1.54 Å and a two-dimensional gas-filled wire array detector (both Molecular Metrology, Inc.) at a distance of 1.476 m from the sample. The raw data were calibrated against the peak position of a silver behenate standard which has a scattering vector of q = 1.076 1/nm. Two-dimensional images were reduced to the one-dimensional form using angular integration. Domain spacings were calculated from the principal scattering maxima (q^*) calculated using $d = 2\pi/q^*$. For TEM analysis, ultra-thin sections were cut on a Leica Ultracut microtome operating at −80 °C, stained with RuO_4 for 10 min, and imaged using a JEOL 2000FX operating at an accelerating voltage of 200 kV. Mechanical properties were tested using dynamic mechanical analysis (DMA) with a TA Instruments DMA Q800. A preload force of 1.0 mN was applied. Samples were stretched to 0.1% strain at a constant frequency of 1 Hz. Measurements were taken from −80 to +130 °C with a heating rate of 3 °C/min.

Conflict of Interest: The authors declare no competing financial interest.

Acknowledgment. This work was supported by the Office of Naval Research (N00014-10-1-0348) and the National Science Foundation through the MRSEC on Polymers at UMass DMR-0820506. We thank B. M. deRonde and C. Backlund for assisting with manuscript preparation, M. A. Lackey for functionalizing the 35 kg/mol PEG, and E. Anderson for assistance obtaining the impedance spectroscopy data.

Supporting Information Available: Materials, methods, precursor polymer characterization, TGA, and additional DSC curves. This material is available free of charge *via* the Internet at http://pubs.acs.org.

REFERENCES AND NOTES

1. Register, R. A. Continuity through Dispersity. *Nature* **2012**, *483*, 167–168.
2. Hickner, M. Ion-Containing Polymers: New Enery and Clean Water. *Mater. Today* **2010**, *13*, 35–41.
3. Matsen, M. W.; Bates, F. S. Origins of Complex Self-Assembly in Block Copolymers. *Macromolecules* **1996**, *29*, 7641–7644.
4. Cochran, E. W.; Garcia-Cervera, C. J.; Fredrickson, G. H. Stability of the Gyroid Phase in Diblock Copolymers at Strong Segregation. *Macromolecules* **2006**, *39*, 2449–2451.
5. Wanakule, N. S.; Panday, A.; Mullin, S. A.; Gann, E.; Hexemer, A.; Balsara, N. P. Ionic Conductivity of Block Copolymer Electrolytes in the Vicinity of Order−Disorder and Order−Order Transitions. *Macromolecules* **2009**, *42*, 5642–5651.
6. Meyer, W. H. Polymer Electrolytes for Lithium Ion Batteries. *Adv. Mater.* **1998**, *10*, 439–448.
7. Thompson, B. C.; Fréchet, J. M. J. Polymer−Fullerene Composite Solar Cells. *Angew. Chem., Int. Ed. Engl.* **2008**, *47*, 58–77.
8. Schultz, C. L.; Morck, D. W. Contact Lenses as a Drug Delivery Device for Epidermal Growth Factor in the Treatment of Ocular Wounds. *Clin. Exp. Optom.* **2010**, *93*, 61–65.
9. Dair, B. J.; Honeker, C.; Alward, D. B.; Avgeropoulos, A.; Hadjichristidis, N.; Fetters, L. J.; Capel, M.; Thomas, E. L. Mechanical Properties and Deformation Behavior of the Double Gyroid Phase in Unoriented Thermoplastic Elastomers. *Macromolecules* **1999**, *32*, 8145–8152.
10. Dair, B. J.; Avgeropoulos, A.; Hadjichristidis, N.; Thomas, E. L. Mechanical Properties of the Double Gyroid Phase in Oriented Thermpolastic Elastomers. *J. Mater. Sci.* **2000**, *35*, 5207–5213.
11. Bates, F. S.; Fredrickson, G. H. Block Copolymers—Designer Soft Materials. *Phys. Today* **1999**, *52*, 32.
12. Matsen, M. W. The Standard Gaussian Model for Block Copolymer Melts. *J. Phys.: Condens. Matter* **2002**, *14*, R21.
13. Bates, F. S.; Fredrickson, G. H. Block Copolymer Thermodynamics: Theory and Experiment. *Annu. Rev. Phys. Chem.* **1990**, *41*, 525.
14. Brown, J. R.; Sides, S. W.; Hall, L. M. Phase Behavior of Tapered Diblock Copolymers from Self-Consistent Field Theory. *ACS Macro Lett.* **2013**, *2*, 1105–1109.
15. Widin, J. M.; Schmitt, A. K.; Schmitt, A. L.; Im, K.; Mahanthappa, M. K. Unexpected Consequences of Block Polydispersity on the Self-Assembly of Aba Triblock Copolymers. *J. Am. Chem. Soc.* **2012**, *134*, 3834–3844.
16. Widin, J. M.; Schmitt, A. K.; Im, K.; Schmitt, A. L.; Mahanthappa, M. K. Polydispersity-Induced Stabilization of a Disordered Bicontinuous Morphology in Aba Triblock Copolymers. *Macromolecules* **2010**, *43*, 7913–7915.
17. Schmitt, A. L.; Mahanthappa, M. K. Polydispersity-Driven Shift in the Lamellar Mesophase Composition Window of PEO-PB-PEO Triblock Copolymers. *Soft Matter* **2012**, *8*, 2294.
18. Schmitt, A. K.; Mahanthappa, M. K. Characteristics of Lamellar Mesophases in Strongly Segregated Broad Dispersity Aba Triblock Copolymers. *Macromolecules* **2014**, *47*, 4346–4356.
19. Pernot, H.; Baumert, M.; Court, F.; Leibler, L. Design and Properties of Co-Continuous Nanostructured Polymers by Reactive Blending. *Nat. Mater.* **2002**, *1*, 54–58.
20. Bates, F. S.; Maurer, W. W.; Lipic, P. M.; Hillmyer, M. A.; Almdal, K.; Mortensen, K.; Fredrickson, G. H.; Lodge, T. P. Polymeric Bicontinuous Microemulsions. *Phys. Rev. Lett.* **1997**, *79*, 849–852.
21. Fredrickson, G. H.; Bates, F. S. Design of Bicontinuous Polymeric Microemulsions. *J. Polym. Sci., Part B: Polym. Phys.* **1997**, *35*, 2775–2786.
22. Lee, I.; Bates, F. S. Synthesis, Structure and Properties of Alternating and Random Poly(Styrene-b-Butadiene) Multiblock Copolymers. *Macromolecules* **2013**, *46*, 4529.
23. Lee, I.; Panthani, T. R.; Bates, F. S. Sustainable Poly(Lactide-b-Butadiene) Multiblock Copolymers with Enhanced Mechanical Properties. *Macromolecules* **2013**, *46*, 7387–7398.
24. Krause, S. Microphase Separation in Block Copolymers. Zeroth Approximation Including Surface Free Energies. *Macromolecules* **1970**, *3*, 84–86.
25. Wu, L.; Cochran, E. W.; Lodge, T. P.; Bates, F. S. Consequences of Block Number on the Order−Disorder Transition and Viscoelastic Properties of Linear (Ab)N Multiblock Copolymers. *Macromolecules* **2004**, *37*, 3360–3368.
26. Lee, I.; Bates, F. S. Synthesis, Structure, and Properties of Alternating and Random Poly(Styrene-B-Butadiene) Multiblock Copolymers. *Macromolecules* **2013**, *46*, 4529–4539.
27. Touris, A.; Lee, S.; Hillmyer, M. A.; Bates, F. S. Synthesis of Tri- and Multiblock Polymers with Asymmetric Poly(Ethylene Oxide) End Blocks. *ACS Macro Lett.* **2012**, *1*, 768–771.
28. Gemici, H.; Legge, T. M.; Whittaker, M.; Monteiro, M. J.; Perrier, S. Original Approach to Multiblock Copolymers Via Reversible Addition−Fragmentation Chain Transfer Polymerization. *J. Polym. Sci., Part A: Polym. Chem.* **2007**, *45*, 2334–2340.

29. Gody, G.; Maschmeyer, T.; Zetterlund, P. B.; Perrier, S. Rapid and Quantitative One-Pot Synthesis of Sequence-Controlled Polymers by Radical Polymerization. *Nat. Commun.* **2013**, *4*, 2505.
30. Walker, C. N.; Sarapas, J. M.; Kung, V.; Hall, A. L.; Tew, G. N. Multiblock Copolymers by Thiol Addition across Norbornene. *ACS Macro Lett.* **2014**, *3*, 453–457.
31. Löwen, H. Solvent-Induced Phase Separation in Colloidal Fluids. *Phys. Rev. Lett.* **1995**, *74*, 1028–1031.
32. Li, L.; Shen, X.; Hong, S. W.; Hayward, R. C.; Russell, T. P. Fabrication of Co-Continuous Nanostructured and Porous Polymer Membranes: Spinodal Decomposition of Homopolymer and Random Copolymer Blends. *Angew. Chem.* **2012**, *51*, 4089–4094.
33. Ozaki, T.; Koto, T.; Nguyen, T. V.; Nakanishi, H.; Norisuye, T.; Tran-Cong-Miyata, Q. The Roles of the Trommsdorff–Norrish Effect in Phase Separation of Binary Polymer Mixtures Induced by Photopolymerization. *Polymer* **2014**, *55*, 1809–1816.
34. Shukutani, T.; Myojo, T.; Nakanishi, H.; Norisuye, T.; Tran-Cong-Miyata, Q. Tricontinuous Morphology of Ternary Polymer Blends Driven by Photopolymerization: Reaction and Phase Separation Kinetics. *Macromolecules* **2014**, *47*, 4380–4386.
35. Hayward, R. C.; Pochan, D. J. Tailored Assemblies of Block Copolymers in Solution: It Is All About the Process. *Macromolecules* **2010**, *43*, 3577–3584.
36. Nam, Y. S.; Park, T. G. Porous Biodegradable Polymeric Scaffolds Prepared by Thermally Induced Phase Separation. *J. Biomed. Mater. Res.* **1999**, *47*, 8–17.
37. Schulze, M. W.; McIntosh, L. D.; Hillmyer, M. A.; Lodge, T. P. High-Modulus, High-Conductivity Nanostructured Polymer Electrolyte Membranes Via Polymerization-Induced Phase Separation. *Nano Lett.* **2014**, *14*, 122–126.
38. Price, S. C.; Ren, X.; Jackson, A. C.; Ye, Y.; Elabd, Y. A.; Beyer, F. L. Bicontinuous Alkaline Fuel Cell Membranes from Strongly Self-Segregating Block Copolymers. *Macromolecules* **2013**, *46*, 7332–7340.
39. Trinh, X.-A.; Fukuda, J.; Adachi, Y.; Nakanishi, H.; Norisuye, T.; Tran-Cong-Miyata, Q. Effects of Elastic Deformation on Phase Separation of a Polymer Blend Driven by a Reversible Photo-Cross-Linking Reaction. *Macromolecules* **2007**, *40*, 5566–5574.
40. Chung, H.-j.; Ohno, K.; Fukuda, T.; Composto, R. J. Self-Regulated Structures in Nanocomposites by Directed Nanoparticle Assembly. *Nano Lett.* **2005**, *5*, 1878–1882.
41. Seo, M.; Hillmyer, M. A. Reticulated Nanoporous Polymers by Controlled Polymerization-Induced Microphase Separation. *Science* **2012**, *336*, 1422–1425.
42. de Gennes, P. G. Effect of Cross-Links on a Mixture of Polymers. *J. Phys., Lett.* **1979**, *40*, L-69–72.
43. Briber, R. M.; Bauer, J. B. Effect of Cross-Links on the Phase Separation Behavior of a Miscible Polymer Blend. *Macromolecules* **1988**, *21*, 3296–3303.
44. Panyukov, S.; Rubinstein, M. Stress-Induced Ordering in Microphase Separated Multicomponent Networks. *Macromolecules* **1996**, *29*, 8220–8230.
45. Ivan, B.; Almdal, K.; Mortensen, K.; Johannsen, I.; Kops, J. Synthesis Characterization and Structural Investigations of Poly(Ethyl Acrylate)-L-Polyisobutylene Bicomponent Conetowork. *Macromolecules* **2001**, *34*, 1579–1585.
46. Bruns, N.; Scherble, J.; Hartmann, L.; Thomann, R.; Iván, B.; Mülhaupt, R.; Tiller, J. C. Nanophase Separated Amphiphilic Conetwork Coatings and Membranes. *Macromolecules* **2005**, *38*, 2431–2438.
47. Haraszti, M.; Toth, E.; Ivan, B. Poly(Methacrylic Acid)-L-Polyisobutylene: A Novel Polyelectrolyte Amphiphiclic Conetwork. *Chem. Mater.* **2006**, *18*, 4952–4958.
48. Fodor, C.; Kali, G.; Iván, B. Poly(*N*-vinylimidazole)-*l*-Poly(tetrahydrofuran) Amphiphilic Conetworks and Gels: Synthesis, Characterization, Thermal and Swelling Behavior. *Macromolecules* **2011**, *44*, 4496–4502.
49. Erdodi, G.; Kennedy, J. P. Amphiphilic Conetworks: Definition, Synthesis, Applications. *Prog. Polym. Sci.* **2006**, *31*, 1–18.
50. Hadjiantoniou, N. A.; Patrickios, C. S.; Thomann, Y.; Tiller, J. C. Amphiphilic Conetworks Based on End-Linked Multiblock Copolymers of Different Numbers of Blocks and Constant Molecular Weight and Composition. *Macromol. Chem. Phys.* **2009**, *210*, 942–950.
51. Kali, G.; Georgiou, T. K.; Ivan, B.; Patrickios, C. S.; Loizou, E.; Thoumann, Y.; Tiller, J. C. Synthesis and Characterization of Anionic Amphiphilic Model Conetworks of 2-Butyl-1-Octyl-Methacrylate and Methacrylic Acid: Effects of Polymer Composition and Architecture. *Langmuir* **2007**, *23*, 10746–10755.
52. Rikkou, M. D.; Kolokasi, M.; Matyjaszewski, K.; Patrickios, C. S. End-Linked Amphiphilic Polymer Conetworks: Synthesis by Sequential Atom Transfer Radical Polymerization and Swelling Characterization. *J. Polym. Sci., Part A: Polym. Chem.* **2010**, *48*, 1878–1886.
53. Singh, M.; Odusanya, O.; Wilmes, G. M.; Eitouni, H. B.; Gomez, E. D.; Patel, A. J.; Chen, V. L.; Park, M. J.; Fragouli, P.; Iatrou, H.; Hadjichristidis, N.; Cookson, D.; Balsara, N. P. Effect of Molecular Weight on the Mechanical and Electrical Properties of Block Copolymers Electrolytes. *Macromolecules* **2007**, *40*, 4578–4585.
54. Nakamura, I.; Balsara, N. P.; Wang, Z.-G.: Thermodynamics of Ion-Containing Polymer Blends and Block Copolymers. *Phys. Rev. Lett.* **2011**, *107*.
55. Yuan, R.; Teran, A. A.; Gurevitch, I.; Mullin, S. A.; Wanakule, N. S.; Balsara, N. P. Ionic Conductivity of Low Molecular Weight Block Copolymer Electrolytes. *Macromolecules* **2013**, *46*, 914–921.
56. Cui, J.; Lackey, M. A.; Tew, G. N.; Crosby, A. J. Mechanical Properties of End-Linked PEG/PDMS Hydrogels. *Macromolecules* **2012**, *45*, 6104–6110.
57. Cui, J.; Lackey, M. A.; Madkour, A. E.; Saffer, E. M.; Griffin, D. M.; Bhatia, S. R.; Crosby, A. J.; Tew, G. N. Synthetically Simple, Highly Resilient Hydrogels. *Biomacromolecules* **2012**, *13*, 584–588.
58. Saffer, E. M.; Lackey, M. A.; Griffin, D. M.; Kishore, S.; Tew, G. N.; Bhatia, S. R. Sans Study of Highly Resilient Poly(Ethylene Glycol) Hydrogels. *Soft Matter* **2014**, *10*, 1905–1916.
59. Gervais, M.; Gallot, B. Phase Diagram and Structural Study of Polystyrene - Poly(Ethylene Oxide) Block Copolymers, 1. *Macromol. Chem. Phys.* **1973**, *171*, 145–178.
60. Walker, C. N.; Versek, C.; Touminen, M.; Tew, G. N. Tunable Networks from Thiolene Chemistry for Lithium Ion Conduction. *ACS Macro Lett.* **2012**, *1*, 737–741.
61. Bates, F. S.; Fredrickson, G. H. Block Copolymer Thermodynamics: Theory and Experiment. *Annu. Rev. Phys. Chem.* **1990**, *41*, 525–557.
62. Cui, J. Resilient Polymer Networks Vi Thiol-Norbornene Chemistry: Mechanical and Adhesive Properties. Doctoral Dissertation, University of Massachusetts Amherst, 2013.
63. Northrop, B. H.; Coffey, R. N. Thiol-Ene Click Chemistry: Computational and Kinetic Analysis of the Influence of Alkene Functionality. *J. Am. Chem. Soc.* **2012**, *134*, 13804–13817.
64. Fairbanks, B. D.; Singh, S. P.; Bowman, C. N.; Anseth, K. S. Photodegradable, Photoadaptable Hydrogels Via Radical-Mediated Disulfide Fragmentation Reaction. *Macromolecules* **2011**, *44*, 2444–2450.
65. Morgan, C. R.; Magnotta, F.; Ketley, A. D. Thiol/Ene Photocuable Polymers. *J. Polym. Sci.: Polym. Chem. Ed* **1977**, *15*, 627–645.
66. Jinnai, H.; Nishikawa, Y.; Koga, T.; Hashimoto, T. Direct Observation of 3-D Bicontinuous Structure Developed Via Spinodal Decomposition. *Macromolecules* **1995**, *28*, 4782–4784.
67. Frielinghaus, H.; Mortensen, K.; Almdal, K. Differences of Interaction Parameter of a Ps/Peo Homopolymer Blend and Diblock Copolymer in Comparison to Other Systems. *Macromol. Symp.* **2000**, *149*, 63–67.
68. Wanakule, N. S.; Virgili, J. M.; Teran, A. A.; Wang, Z.-G.; Balsara, N. P. Thermodynamic Properties of Block Copolymer Electrolytes Containing Imidazolium and Lithium Salts. *Macromolecules* **2010**, *43*, 8282–8289.

69. Nakamura, I.; Balsara, N. P.; Wang, Z.-G. First-Order Disordered-to-Lamellar Phase Transition in Lithium Salt-Doped Block Copolymers. *ACS Macro Lett.* **2013**, *2*, 478–481.
70. Kono, M.; Hayashi, E.; Watanabe, M. Network Polymer Electrolytes with Free Chain Ends as Internal Plasticizer. *J. Electrochem. Soc.* **1998**, *145*, 1521–1527.
71. Rossi, N. A. A.; Z, Z.; Schneider, Y.; Morcom, K.; Lyons, L. J.; Wang, Q.; Amine, K.; West, R. Synthesis and Characterization of Tetra- and Trisiloxane-Containing Ologio(Ethylene Glycol)s - Highly Conducting Electrolytes for Lithium Batteries. *Chem. Mater.* **2006**, *18*, 1289–1295.
72. Oh, B.; Vissers, D.; Zhang, Z.; West, R.; Tsukamoto, H.; Amine, K. New Interpenetrating Network Type Poly-(Siloxane-g-Ethylene Oxide) Polymer Electrolyte for Lithium Battery. *J. Power Sources* **2003**, *119−121*, 442–447.
73. Panday, A.; Mullin, S.; Gomez, E. D.; Wanakule, N.; Chen, V. L.; Hexemer, A.; Pople, J.; Balsara, N. P. Effect of Molecular Weight and Salt Concentration on Conductivity of Block Copolymer Electrolytes. *Macromolecules* **2009**, *42*, 4632–4637.
74. Tigelaar, D. M.; Meador, M. A. B.; Kinder, J. D.; Bennett, W. R. New Aptes Cross-Linked Polymers from Poly(Ethylene Oxide)s and Cyanuric Chloride for Lithium Batteries. *Macromolecules* **2006**, *39*, 120–127.
75. Halalay, I. C.; Lukitsch, M. J.; Balogh, M. P.; Wong, C. A. Nanoindentation Testing of Separators for Lithium-Ion Batteries. *J. Power Sources* **2013**, *238*, 469–477.